AD-A124 300 DETERMINATION OF AL IN GA(1-X)AL(X)AS BY AUGER SPECTROSCOPY ION MICROPROB.. (U) AEROSPACE CORP EL SEGUNDO CA ELECTRONICS RESEARCH LAB T S STEWART ET AL. 1/1

UNCLASSIFIED 06 DEC 82 TR-0083(3925-01)-3 SD-TR-82-90 F/G 7/4 NL

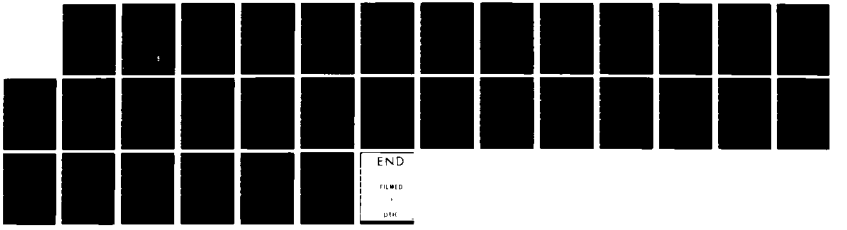

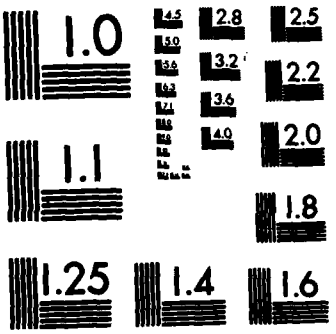

Determination of Al in $Ga_{1-x}Al_xAs$ by Auger Spectroscopy, Ion Microprobe Mass Analysis, and Photoluminescence

T. S. STEWART
Hewlett-Packard
Corvallis, Ore. 97330

S. I. BOLDISH, J. A. OSMER,
N. MARQUEZ, and D. G. HEFLINGER
Electronics Research Laboratory
Laboratory Operations
The Aerospace Corporation
El Segundo, Calif. 90245

G. A. EVANS and J. B. KIRK
TRW Systems and Energy
Redondo Beach, Calif. 90278

A. CERUZZI, A. MANTIE, and T. STOCKTON
Laser Diode Laboratories
New Brunswick, N. J. 08901

6 December 1982

Prepared for

SPACE DIVISION
AIR FORCE SYSTEMS COMMAND
Los Angeles Air Force Station
P.O. Box 92960, Worldway Postal Center
Los Angeles, Calif. 90009

This report was submitted by The Aerospace Corporation, El Segundo, CA 90245, under Contract No. F04701-82-C-0083 with the Space Division, Deputy for Technology, P.O. Box 92960, Worldway Postal Center, Los Angeles, CA 90009. It was reviewed and approved for The Aerospace Corporation by D. H. Phillips, Director, Electronics Research Laboratory. Lt R. R. Herndon, SD/YLXT, was the project officer for the Mission-Oriented Investigation and Experimentation (MOIE) Program.

This report has been reviewed by the Public Affairs Office (PAS) and is releasable to the National Technical Information Service (NTIS). At NTIS, it will be available to the general public including foreign nations.

This technical report has been reviewed and is approved for publication. Publication of this report does not constitute Air Force approval of the report's findings or conclusions. It is published only for the exchange and stimulation of ideas.

Russell R. Herndon, 2nd Lt, USAF
Project Officer

David T. Newell, Lt Colonel, USAF
Actg Dir of Space Systems Technology

FOR THE COMMANDER

Norman W. Lee, Jr., Colonel, USAF
Commander, Det 1, AFSTC

UNCLASSIFIED

SECURITY CLASSIFICATION OF THIS PAGE (When Data Entered)

REPORT DOCUMENTATION PAGE	READ INSTRUCTIONS BEFORE COMPLETING FORM
1. REPORT NUMBER: SD-TR-82-90	2. GOVT ACCESSION NO.: AD-A124 365
	3. RECIPIENT'S CATALOG NUMBER:
4. TITLE (and Subtitle): DETERMINATION OF Al IN $Ga_{1-x}Al_xAs$ BY AUGER SPECTROSCOPY, ION MICROPROBE MASS ANALYSIS, AND PHOTOLUMINESCENCE	5. TYPE OF REPORT & PERIOD COVERED:
	6. PERFORMING ORG. REPORT NUMBER: TR-0083(3925-01)-3
7. AUTHOR(s): T. S. Stewart, S. I. Boldish, J. A. Osmer, N. Marquez, D. G. Heflinger, G. A. Evans, J. B. Kirk, A. Ceruzzi, A. Mantie, and T. Stockton	8. CONTRACT OR GRANT NUMBER(s): F04701-82-C-0083
9. PERFORMING ORGANIZATION NAME AND ADDRESS: Laboratory Operations, The Aerospace Corporation, El Segundo, Calif. 90245	10. PROGRAM ELEMENT, PROJECT, TASK AREA & WORK UNIT NUMBERS:
11. CONTROLLING OFFICE NAME AND ADDRESS: Space Division, Air Force Systems Command, Los Angeles, Calif. 90009	12. REPORT DATE: 6 December 1982
	13. NUMBER OF PAGES: 27
14. MONITORING AGENCY NAME & ADDRESS (if different from Controlling Office):	15. SECURITY CLASS. (of this report): Unclassified
	15a. DECLASSIFICATION/DOWNGRADING SCHEDULE:

16. DISTRIBUTION STATEMENT (of this Report)

Approved for public release; distribution unlimited.

17. DISTRIBUTION STATEMENT (of the abstract entered in Block 20, if different from Report)

18. SUPPLEMENTARY NOTES

19. KEY WORDS (Continue on reverse side if necessary and identify by block number)

Auger spectroscopy	IMMA
Chemical analysis	Liquid phase epitaxial growth
$Ga_{1-x}Al_xAs$	Photoluminescence
Gallium aluminum arsenide	Secondary ion mass spectroscopy
Ion microprobe mass analysis	SIMS

20. ABSTRACT (Continue on reverse side if necessary and identify by block number)

Single layers of $Ga_{1-x}Al_xAs$ were grown on semi-insulating Cr-doped GaAs substrates by liquid phase epitaxy. The samples consisted of six series. Within each series, the mole fraction of Al ranged from 0 to 0.45. Each series was either doped p with Ge or n with Te. The doping levels ranged from 10^{15} to 10^{19} carriers/cm^3. The mole fraction of Al in each sample was measured independently by Auger electron spectroscopy, ion microprobe mass analysis, and photoluminescence for comparison with phase diagram predictions. The carrier

DD FORM 1473 (FACSIMILE)

UNCLASSIFIED

SECURITY CLASSIFICATION OF THIS PAGE (When Data Entered)

19. KEY WORDS *(Continued)*

20. ABSTRACT *(Continued)*

concentrations were estimated by the half-width of the photoluminescence peaks. The techniques, and their discrepancies and agreements, are discussed.

CONTENTS

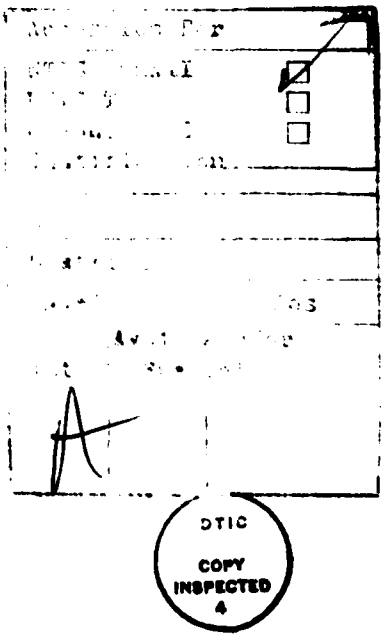

FIGURES

TABLE

I. INTRODUCTION

The development of new $Ga_{1-x}Al_xAs$ heterostructure laser devices has received considerable attention during the past few years. The successful fabrication of these devices requires considerable skill to control the Al concentrations in $Ga_{1-x}Al_xAs$ during epitaxial growth. Knowledge of the mole fraction of Al in epitaxial layers of the laser devices is necessary since the laser frequency and waveguide confinement are dependent upon it.

Al concentration is most often measured by photoluminescence or electron microprobe mass analysis. The results produced by these methods are not very accurate. For photoluminescence the spectral line shifts with the amount of p or n dopant, and for the electron microprobe the correction factor is uncertain because of matrix effects. Most photoluminescence curves and phase diagrams give the Al concentration from electron microprobe data, which compounds the uncertainty.

This report discusses and compares the quantitative determination of Al by Auger electron spectroscopy, ion microprobe mass analysis (IMMA), and photoluminescence for six series of single-layer $Ga_{1-x}Al_xAs$ grown by liquid phase epitaxy (LPE) on Cr-doped GaAs substrates and compares the results with phase diagram predictions. Within each series the mole fraction of Al varied from 0 to 0.45. The layers in each series were grown doped either p with Ge or n with Te or were left undoped. Within each series, the amount of dopant added to the melt was kept constant.

II. CRYSTAL GROWTH

Samples were provided by Laser Diode Laboratories, Inc., and were grown by the liquid phase epitaxial technique. A conventional, horizontal, multibin slider boat system was used to grow the single layers.[1-4] The substrates were semi-insulating with Cr-dopant and polished on the (100) face. The weights of Al plus GaAs sufficient to saturate a gallium melt at 800°C were determined from phase diagrams; weights of p-dopant Ge or n-dopant Te added to the melt to yield specific free carrier concentrations were determined from plots of dopant concentration versus free carrier concentration.[5-9] The melts were soaked at 815°C for 2 hr to aid in the dissolution of all material. The melts were then lowered to 800°C, at which point the substrates were placed under the melt and growth was initiated by cooling the furnace at 0.25°C/min for a total temperature drop of 4°C.

The measured Al concentration in some layers was much less than the predicted phase diagram values. The most likely explanation is that not all of the Al was dissolved since the dissolution rate of Al is slow in saturated GaAs melts.

III. AUGER ANALYSIS

The use of Auger electron spectroscopy to measure Al quantitatively in $Ga_{1-x}Al_xAs$ is based on the work of Arthur and LePore, who have examined extensively the $Ga_{1-x}Al_xAs$ system.[10]

The Auger process yields an ejected electron from an atom with a characteristic kinetic energy. The process is started by the removal of a core electron by an x-ray photon or high-energy electron, which places the atom in an unstable high-energy state. To release this energy, an electron drops from a higher-energy level to the partially empty core level. The electron transfer results in one of two competing energy-releasing processes: (1) the emission of an x-ray photon or (2) the ejection of an Auger electron. For atoms with atomic numbers lower than 40, the ejection of an Auger electron is the dominant process.

Auger measurements were made with a Perkin-Elmer model 590 scanning Auger microprobe. A 5-kV electron beam at 3×10^{-6} A incident upon the sample surface caused emission of Auger electrons. The incident beam diameter was held to 3 μm. The samples were sputtered initially with a 2-kV Ar ion beam at 25 mA to remove the surface oxide. Then the ion beam was reduced to 5 mA. Surface oxides were formed continuously while the Auger measurements were being taken. It was necessary to measure the Auger spectra during the Ar ion etching to prevent interference from these oxides with the measurements. All samples were aligned carefully at the focal point of the Auger analyzer. This alignment eliminated any instrumental effects, made measurements reproducible, and ensured proper peak-to-peak height ratios. Possible electron beam damage was measured by monitoring changes in Ga, Al, and As Auger intensities while stepping the beam across the surface. There were no significant Auger intensity changes, which indicated that no significant electron-beam-induced surface damage occurred. The Auger analyses of the layers were accomplished with the 1070- and 55-eV Auger electrons of Ga, the 1228- and 43-eV Auger electrons of As, and the 1396-eV Auger electrons of Al. The samples were analyzed repeatedly during a six-month period to establish the reproducibility and precision of the Auger measurements.

The precision of quantitative Auger measurements is dependent upon surface contamination and the inelastic mean free path (IMFP) for the Auger electrons. Overlayers of any contaminant effectively scatter the Auger electron as it reaches the surface from the bulk and reduce the Auger signal. The IMFP is the distance an electron travels before it is scattered. It is approximately independent of the matrix for all inorganic solids but is directly dependent upon the kinetic energy of the Auger electron; consequently, the low-energy electrons have a much lower IMFP than high-energy electrons. The IMFPs for Ga, Al, and As electrons were computed from an empirically derived analytical expression for inorganic solids,[11]

$$\lambda(\text{Å}) = \frac{6410}{E^2} + 0.96\ E^{1/2} \qquad (1)$$

where λ is the IMFP and E is the energy for the Auger electron.

The calculated IMFPs for 55-eV Ga and 43-eV As are 9 and 10 Å, respectively. The IMFPs for the high-energy 1070-eV Ga and the 1228-eV As Auger electrons are 31 and 34 Å, respectively. The 1396-eV Al Auger electron has a mean free path of 36 Å. The high-energy 1070-eV Ga, 1228-eV As, and 1396-eV Al Auger electrons were used for a quantitative determination of Al in the $Ga_{1-x}Al_xAs$ layers because of their long mean free paths.

The elimination of oxide from the $Ga_{1-x}Al_xAs$ surface is essential for the precise quantitative determination of Al. Substantial changes in the ratio of Ga to As occur when an oxide is present on the surface. Careful examination of the Ga Auger electron spectrum of a GaAs sample oxidized for specified lengths of time reveals a potential problem. Figure 1 shows a composite of three Auger spectra of Ga in GaAs after different oxygen exposure times. The ordinate in this figure represents the derivative of the product of the number of electrons N at energy E, N(E), times the energy of those electrons. A freshly Ar-sputtered GaAs surface yields a Ga Auger electron peak at 1070 eV that is quite sharp, with a relatively large peak-to-peak height. Oxidation

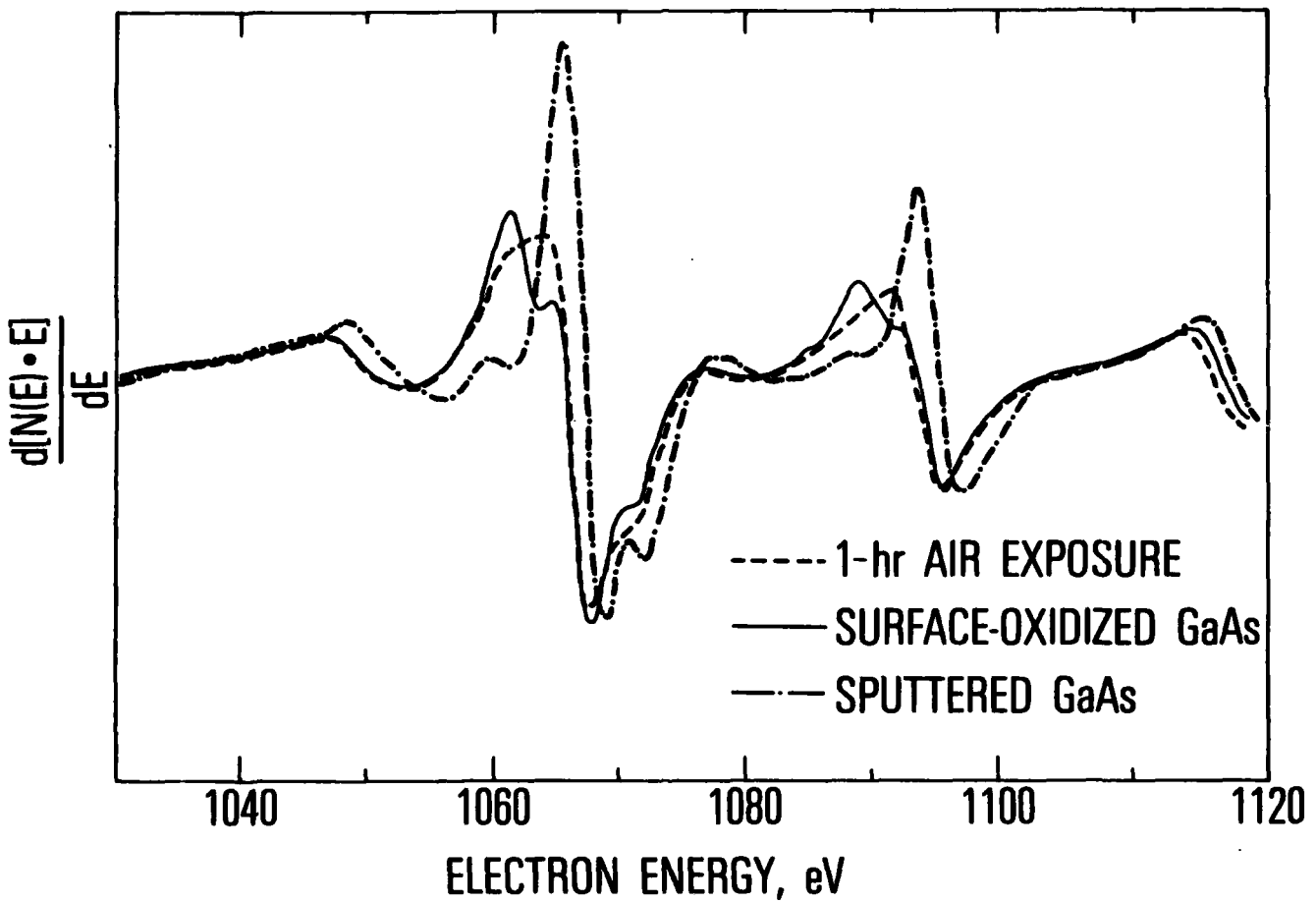

Figure 1. Comparison of Auger spectra for unoxidized (sputtered) GaAs, GaAs oxidized briefly by background gas in the vacuum, and air-oxidized GaAs to show their degradation with oxidation.

reduces the peak-to-peak height intensity and shifts the peak to a lower energy. Slight oxygen exposure doubles the peak and indicates the presence of two Ga oxidation states or the presence of Ga in two chemically different environments. Such chemical shifts were not observed for As.

Arthur and LePore's work used the Ga/As and Al/As peak-to-peak height ratios, the Ga/Al sensitivity factors, and As as an internal standard with a mole fraction of 0.5. They found the Al concentration in $Ga_{1-x}Al_xAs$ layers, with a standard deviation of ±3-4%.[10]

The equations that determine the Al to Ga sensitivity factors are

$$\frac{I_{Ga}}{I_{As}} = \frac{\alpha_{As}}{\alpha_{Ga}} - \frac{\alpha_{Al} I_{Al}}{\alpha_{Ga} I_{As}} \tag{2}$$

$$\frac{\alpha_{As}}{\alpha_{Ga}} = \frac{I^{o}_{Ga}}{I^{o}_{As}} \tag{3}$$

where I_i is the peak-to-peak height intensity of element i, α_i is the sensitivity factor for element i where i is either Ga, Al, or As, and I^{o}_{Ga}/I^{o}_{As} is the ratio of Ga to As peak-to-peak height intensities for pure GaAs. A plot of I_{Ga}/I_{As} versus I_{Al}/I_{As} yields α_{As}/α_{Ga} as the intercept and $-\alpha_{Al}/\alpha_{Ga}$ as the slope. The Al concentration is then calculated by

$$X_{AlAs} = \left(1 + \frac{\alpha_{Ga}}{\alpha_{Al}} \frac{I_{Ga}}{I_{Al}}\right)^{-1} \tag{4}$$

where X is the AlAs mole fraction in $Ga_{1-x}Al_xAs$. Equation (4) does not rely on primary standards to calculate the Al composition.

An Auger spectrum of sample AlX-6 is shown in Figure 2. The Al peak and the low- and high-energy Ga peaks do not overlap or interfere with each other. The close proximity of the Ga, As, and Al high-energy peaks greatly

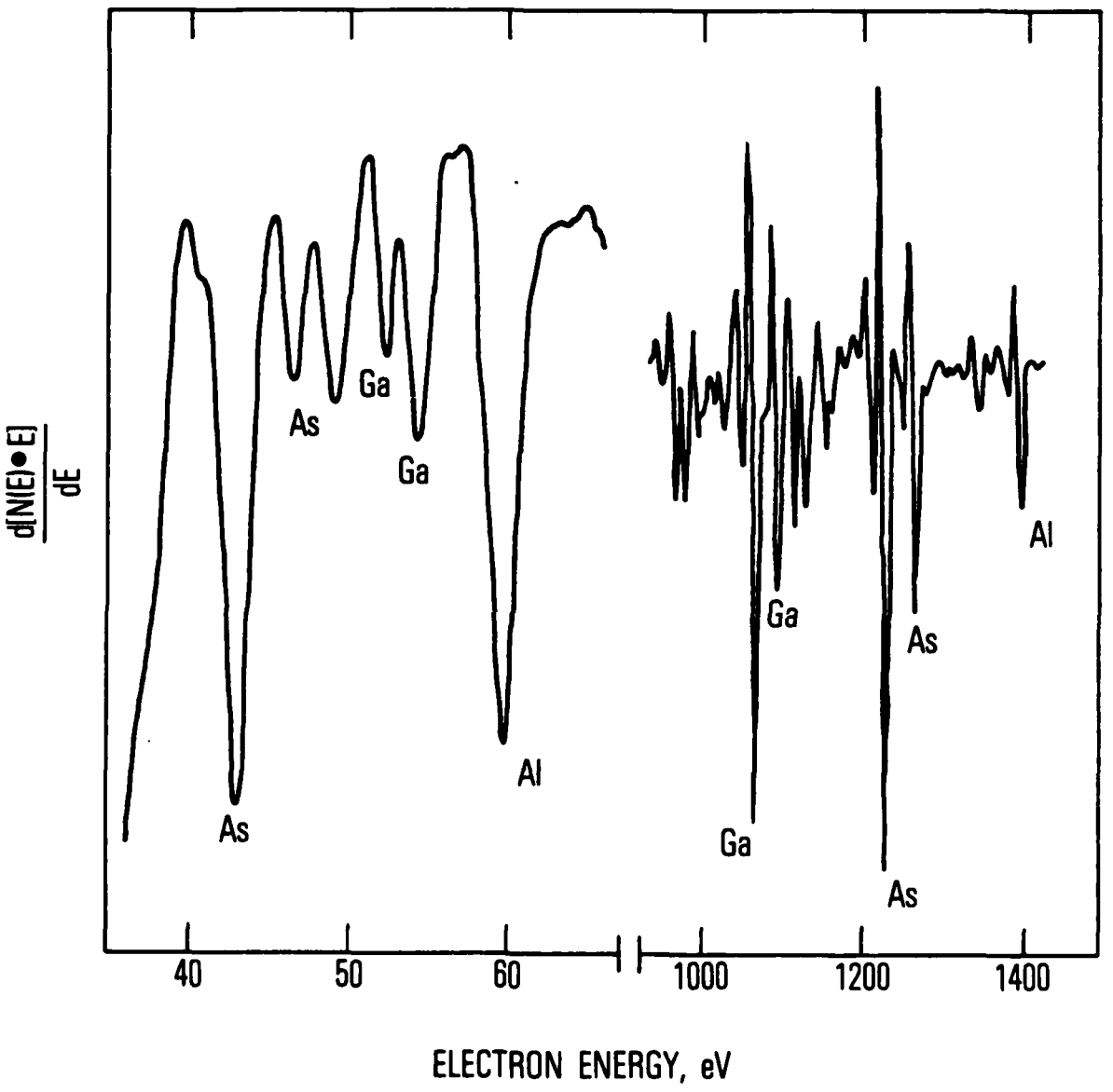

Figure 2. High- and low-energy Auger spectra for sample AlX-6.

reduces errors in the peak-to-peak height intensity ratios. Such errors are caused by surface or instrumental effects and are usually energy dependent. Hence, the closely spaced peaks have their peak-to-peak height intensities equally affected by instrumental factors.

A plot of the Ga/As peak-to-peak height ratio versus Al/As peak-to-peak height ratio is shown in Figure 3. Each datum point is an average of at least 3 and, in some cases, as many as 12 Auger measurements taken on each sample over a period of several months. The uncertainty in each point is the 95% confidence limit calculated from a Student's t-distribution.[12] A linear regression analysis of the data points produces a least squares fit with a slope of -2.87 and an intercept of 1.61. This intercept value is somewhat lower than the value of 1.69 reported by Arthur and LePore;[10] however, it is in the range reported by Ludeke et al. and Van Oostrom, who have reported values of 1.57 and 1.55, respectively.[13,14] The correlation coefficient calculated from linear regression analysis is $r = -0.99$, which indicates a good fit.

Because the Auger measurements and Ar ion sputtering occurred simultaneously, the effects of preferential sputtering on Auger intensities and the Al analysis were considered. This was done by plotting the high-energy versus the low-energy I_{Ga}/I_{As} ratios for samples with different mole fractions of Al. Such a plot is presented in Figure 4. The plot yields a straight line, which indicates that the Ga to As sputtering rate ratio did not change with Al composition. Evidence of preferential sputtering cannot be shown by the plot; however, Van Oostrom reported the preferential sputtering of As over Ga with a sputtering rate ratio of $S_{Ga}/S_{As} = 0.78$.[14]

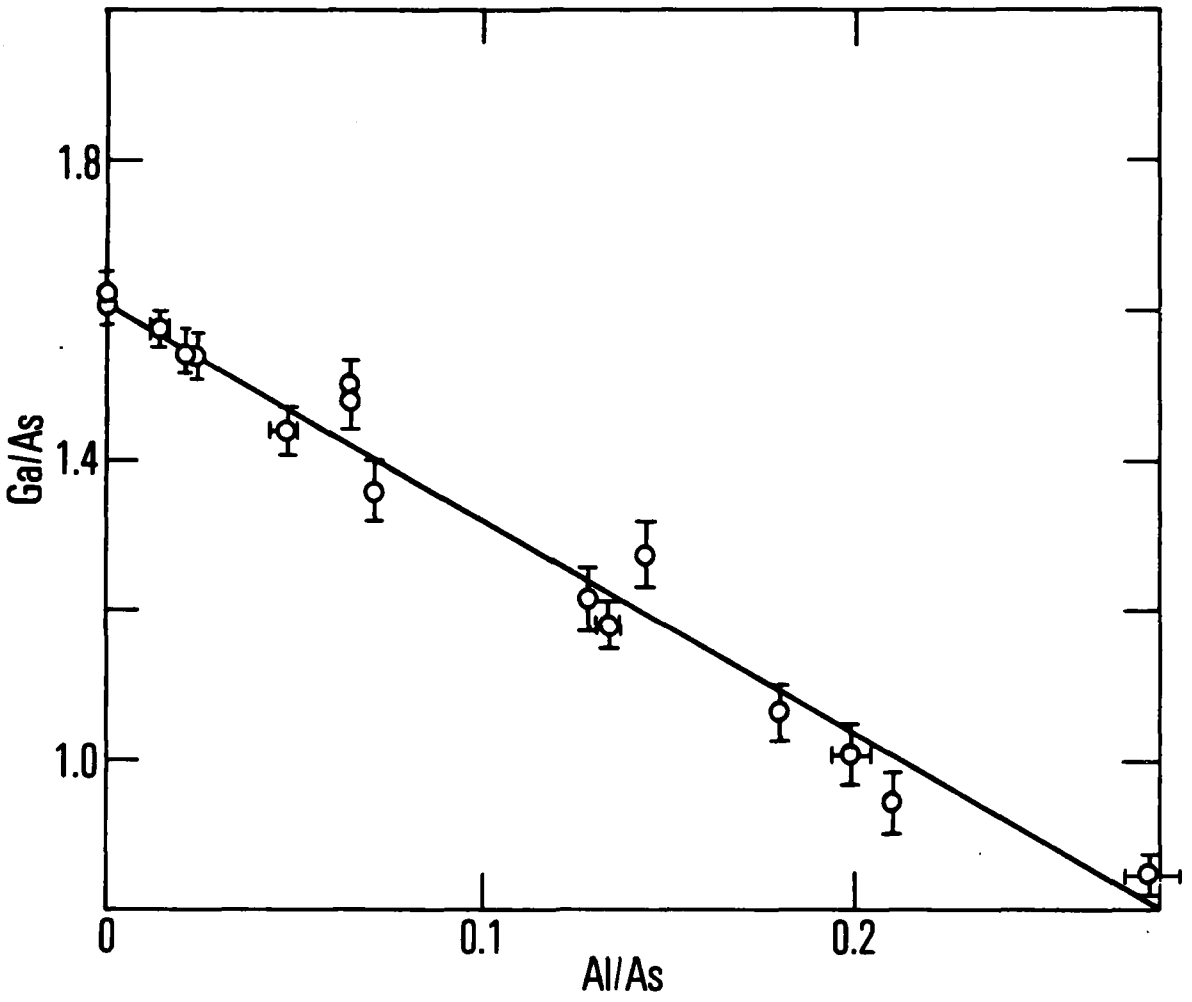

Figure 3. Plot of Ga/As versus Al/As peak-to-peak height ratios for various $Ga_{1-x}Al_xAs$ samples yields a straight line with a slope of -2.87 and an intercept of 1.61. Error bars around data points indicate error limits with 95% confidence.

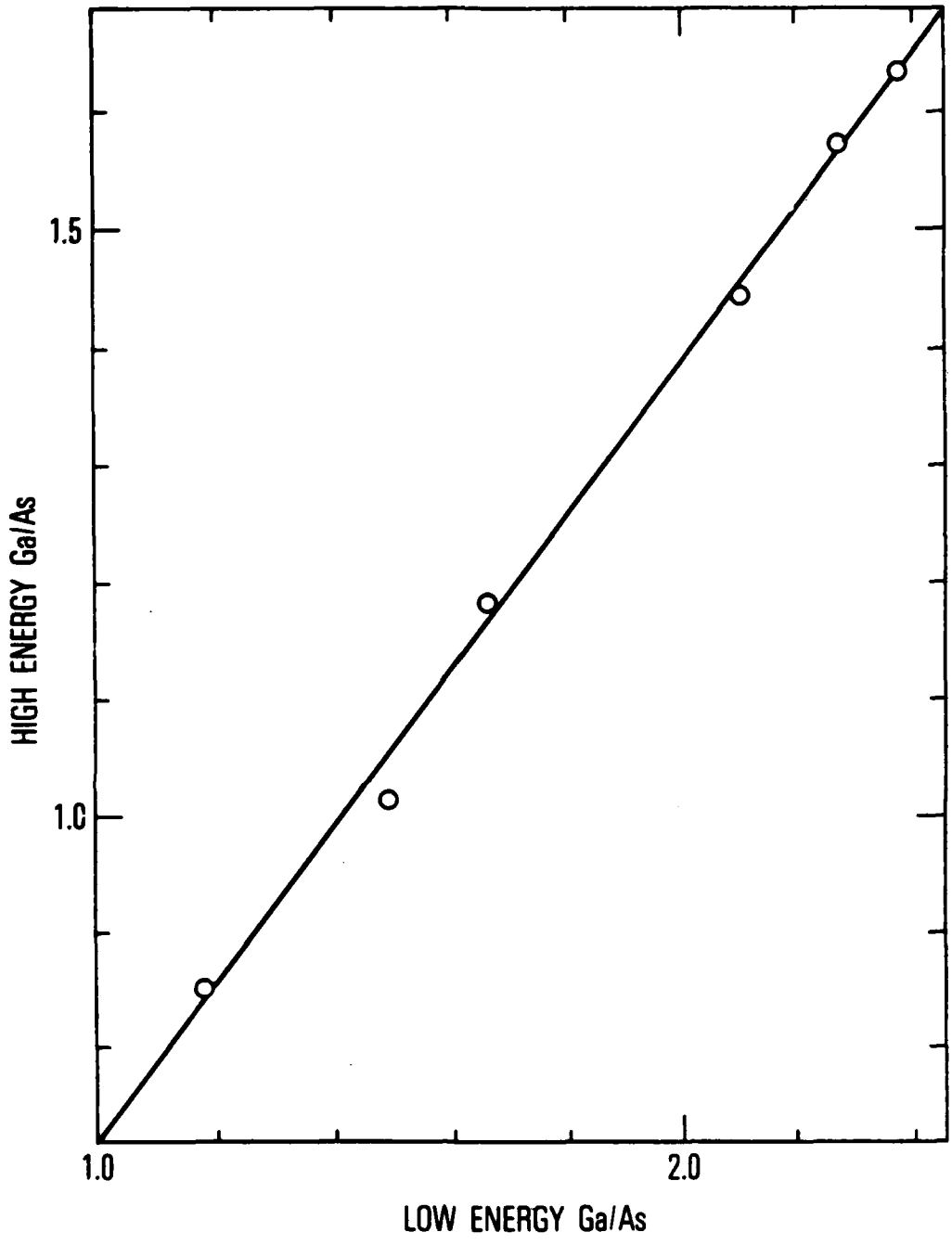

Figure 4. Plot of high-energy Ga/As versus low-energy Ga/As peak-to-peak height ratios yields a straight line with a slope of 0.66 and an intercept of 0.059.

IV. ION MICROPROBE MASS ANALYSIS

An Applied Research Laboratory ion microprobe mass analyzer (IMMA) was used to determine quantitatively the amounts of Al in the single layers of $Ga_{1-x}Al_xAs$. Intensities of singly positive ions of ^{69}Ga, ^{27}Al, and ^{75}As were detected with a scintillation counter. These ions were created by sputtering normal to the epitaxial layers with a $^{18}O_2^+$ molecular-ion beam.

Care was taken to avoid sample charging effects. Ohmic contacts were first made to each of the $Ga_{1-x}Al_xAs$ layers by scrubbing an In preform on each of the epitaxial layers at 170°C to break the surface oxide and to ensure that the In wetted the $Ga_{1-x}Al_xAs$ surface. The samples were then heated to 400°C in flowing N_2 for 5 min to alloy the In to the $Ga_{1-x}Al_xAs$. Next, the samples were mounted on a stainless-steel block with silver paint. Silver paint was also used to make electrical contact from the In dot to the block. This technique eliminated sample charging phenomena, which were found to adversely affect the IMMA analyses.

$^{18}O_2^+$ molecular ions were accelerated by an 18.5-kV potential, striking the sample and inducing it to emit secondary ions. A 0.4-nA oxygen beam current with a 2-μm diameter was used for all analyses. The low incident ion current eliminated saturation of the scintillation counter. The ion beam was rastered for 900 sec over a 25 μm × 20 μm area, but only ions sputtered from a 6 μm × 5 μm area centered on the rastered area were collected as data. Thus, spurious effects in the signal caused by the walls of the rastered hole were eliminated.

Figure 5 contains plots of $^{75}Al^+$, $^{69}Ga^+$, and $^{27}As^+$ raw ion current data obtained from sample MCW 4-4, which are typical of data taken with IMMA. Two important points are illustrated:

1. A surface oxide layer on the $Ga_{1-x}Al_xAs$ samples must be sputtered away to obtain true values for the quantities of Ga, Al, and As in the epitaxial layers.

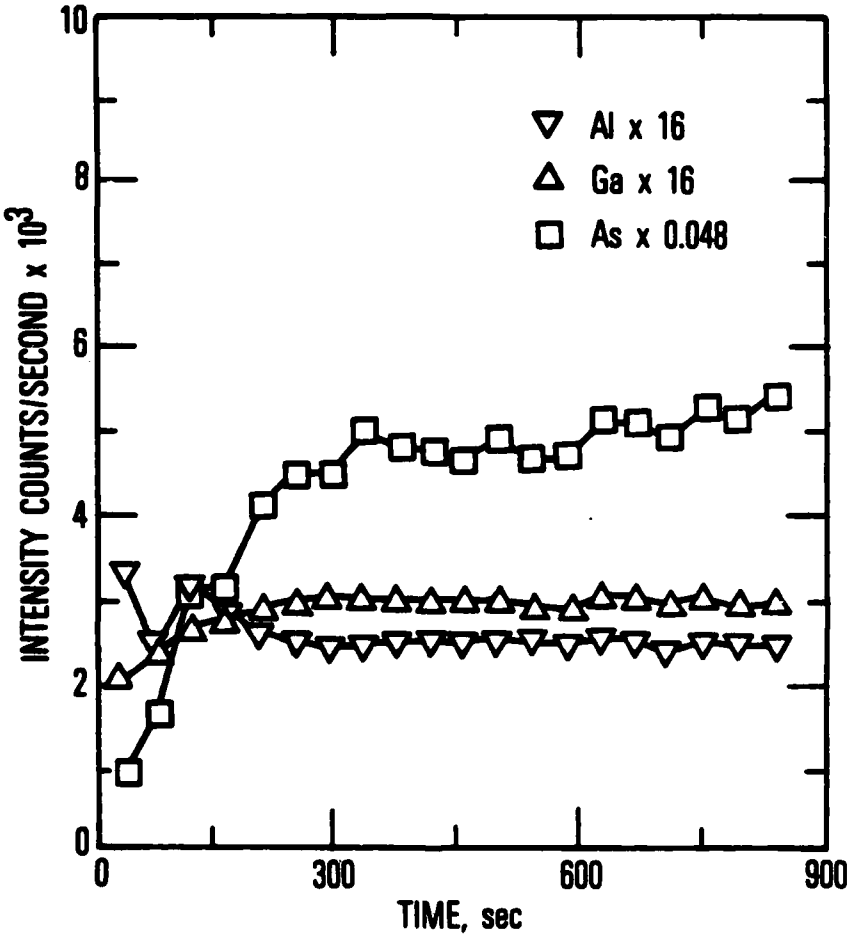

Figure 5. $^{69}Ga^+$, $^{27}Al^+$, and $^{75}As^+$ ion intensities as a function of $^{18}O_2^+$ sputter etch time for MCW 4-4. The scaled ion intensities must be multiplied by the indicated scale factors to obtain actual ion intensities.

2. The Ga^+ and Al^+ secondary ion currents are in the 10^4-counts/sec range, whereas the As^+ secondary ion current is in the 10^2 range. (The secondary ion current data have been multiplied by scale factors to illustrate the data more clearly.)

The existence of the oxide coating is demonstrated by the shapes of the three secondary ion current curves. In the initial stage of sputtering, Ga^+, Al^+, and As^+ ion currents are low. As the sputtering continues, there is a gradual rise for all three secondary ion currents. Once the oxide-$Ga_{1-x}Al_xAs$ interface is reached, the curves bend and gradually flatten, reaching a plateau when sputtering is beyond the interface.

The strong $^{75}Al^+$ and $^{69}Ga^+$ signals and relatively weak $^{27}As^+$ signal result from the almost equal but relatively low electronegativities of Al and Ga and the relatively high electronegativity of As. Thus, Al and Ga easily take on a positive charge, whereas As easily takes on a negative charge and therefore resists becoming positive.

Quantitative values of Al, Ga, and As in the epitaxial layers were derived from the flattened portions of the Ga, Al, and As intensity curves by two techniques. In the first technique the Al and Ga raw data and the relative values of the Ga to Al sensitivity factors α_{Ga}/α_{Al} were needed to determine the Ga to Al ratio in the epitaxial layers. The ratio of the sensitivity factors α_{Ga}/α_{Al} was determined by

$$\frac{\alpha_{Ga}}{\alpha_{Al}} = \frac{C^s_{Ga}}{C^s_{Al}} \cdot \left(\frac{Al}{Ga}\right)_s \qquad (5)$$

where $(Al/Ga)_s$ is the ratio of Al to Ga in the standard epitaxial layer and C^s_{Ga}/C^s_{Al} is a ratio of the Ga^+ to Al^+ secondary ion intensities determined for the standard. Sample MCW 1-5 was chosen as a standard, and its $(Al/Ga)_s$

was determined by Auger analysis to be 32.9/67.1. The ratio α_{Ga}/α_{Al} was found to be 0.478.

The Al to Ga ratio was then determined for each of the layers from the following equation:

$$\frac{Al}{Ga} = \frac{C_{Al}/\alpha_{Al}}{C_{Ga}/\alpha_{Ga}} = \frac{C_{Al}}{C_{Ga}} \cdot \frac{\alpha_{Ga}}{\alpha_{Al}} \tag{6}$$

where C_{Al}/C_{Ga} represents the Al to Ga ion intensities for any sample.

The mole fraction of AlAs in a $Ga_{1-x}Al_xAs$ layer is then given by

$$X_{AlAs} = \left(1 + \frac{C_{Ga}}{C_{Al}} \frac{\alpha_{Al}}{\alpha_{Ga}}\right)^{-1} \tag{7}$$

The second technique used the Al, Ga, and As ion intensity data, and again sample MCW 1-5 was the standard. This technique, however, relies on the relative sensitivity factors for Ga/Al and Ga/As. Equations (5) and (9) were necessary to solve for these relative sensitivity factors. Equation (9) resulted naturally from the definition of the IMMA sensitivity factors in Eq. (8) and from the fact that $Ga_{1-x}Al_xAs$ always has 50% As:

$$\frac{C^s_{As}/\alpha_{As}}{C^s_{Al}/\alpha_{Al} + C^s_{Ga}/\alpha_{Ga} + C^s_{As}/\alpha_{As}} = 0.5 \tag{8}$$

$$\frac{C^s_{As}(\alpha_{Ga}/\alpha_{As})}{C^s_{Al}(\alpha_{Ga}/\alpha_{Al}) + C^s_{Ga} + C^s_{As}(\alpha_{Ga}/\alpha_{As})} = 0.5 \tag{9}$$

The relative sensitivity factors α_{Ga}/α_{As} and α_{Ga}/α_{Al} were determined to be 322 and 0.476, respectively. The atomic fraction η for Al, Ga, and As was determined from

$$\eta_{Ga} = \frac{C_{Ga}}{Z} \tag{10a}$$

$$\eta_{Al} = \frac{C_{Al}}{Z}\left(\frac{\alpha_{Ga}}{\alpha_{Al}}\right) \tag{10b}$$

$$\eta_{As} = \frac{C_{As}}{Z}\left(\frac{\alpha_{Ga}}{\alpha_{As}}\right) \tag{10c}$$

where

$$Z = C_{Al}\left(\frac{\alpha_{Ga}}{\alpha_{Al}}\right) + C_{Ga} + C_{As}\left(\frac{\alpha_{Ga}}{\alpha_{As}}\right)$$

The AlAs mole fraction is then given as

$$X_{AlAs} = 2\eta_{Al} \tag{11}$$

Methods I and II were applied to the single-layer samples. Al concentrations calculated by method I are listed in Table 1. In most cases, the IMMA results are comparable to Auger or photoluminescence results.

Figure 6 contains plots of Al, Ga, and As concentrations calculated by method II as a function of sputter etch time for samples MCW 1-4 and MCW 4-4, with similar Al concentrations. The 50% lines have been included to call attention to the deviation of the calculated As concentration from stoichiometry by as much as 5%.

The use of As data introduces inaccuracies into the calculations because of three problems:

TABLE 1. PERCENTAGE OF AlAs IN SINGLE LAYERS OF $Ga_{1-x}Al_xAs$ PHASE DIAGRAMS DETERMINED BY PHOTOLUMINESCENCE, AUGER SPECTROSCOPY, AND ION MICROPROBE MASS ANALYSIS

Series Title	Sample No.	mg Al/ gm Ga	Phase Diagram, %	Photoluminescence, %	Auger Spectroscopy, %	Ion Microprobe, %
ALX: undoped	1	0	0	—	—	—
	2	0.135	5-8	2	3	4
	3	0.334	21-22	7	9	8
	4	0.668	32-35	20	24	26
	5	1.002	43-45	31	35	37
	6	1.333	50-52	41	49	49
MCW 1: $p = 10^{19}/cm^3$ Ge = 200 mg/gm Ga	1	0	0	—	—	—
	2	0.135	5-8	5	5.2	6
	3	0.334	21-22	9	11.7	12
	4	0.668	32-35	19	22.7	22
	5	1.002	43-45	30	32.9	33
MCW 2: $p = 10^{18}/cm^3$ Ge = 100 mg/gm Ga	1	0	0	—	—	—
	2	0.135	5-8	5	4.1	5
	3	0.335	21-22	12	11.3	14
	4	0.666	32-35	23	23.6	25
	5	1.000	43-45	31	34.2	33
MCW 3: $p = 10^{17}/cm^3$ Ge = 5 mg/gm Ga	1	0	0	—	—	—
	2	0.133	5-8	4	4.3	5
	3	0.333	21-22	10	11.3	13
	4	0.666	32-35	23	15.3	28
	5	1.000	43-45	32	33.2	39
MCW 4: $n = 10^{16}/cm^3$ Te = 0.8 mg/gm Ga	1	0	0	—	—	—
	2	0.134	5-8	4	3.8	5
	3	0.335	21-22	12	12.9	14
	4	0.667	32-35	20	24.5	28
	5	1.000	43-45	26	39.1	41
MCW 5: $n = 10^{19}/cm^3$ Te = 0.8 mg/gm Ga	1	0	0	—	—	—
	2	0.134	5-8	3	3.4	4.5
	3	0.335	21-22	9	11.0	14
	4	0.668	32-35	15	21.0	26
	5	0.998	43-45	29	37.7	45

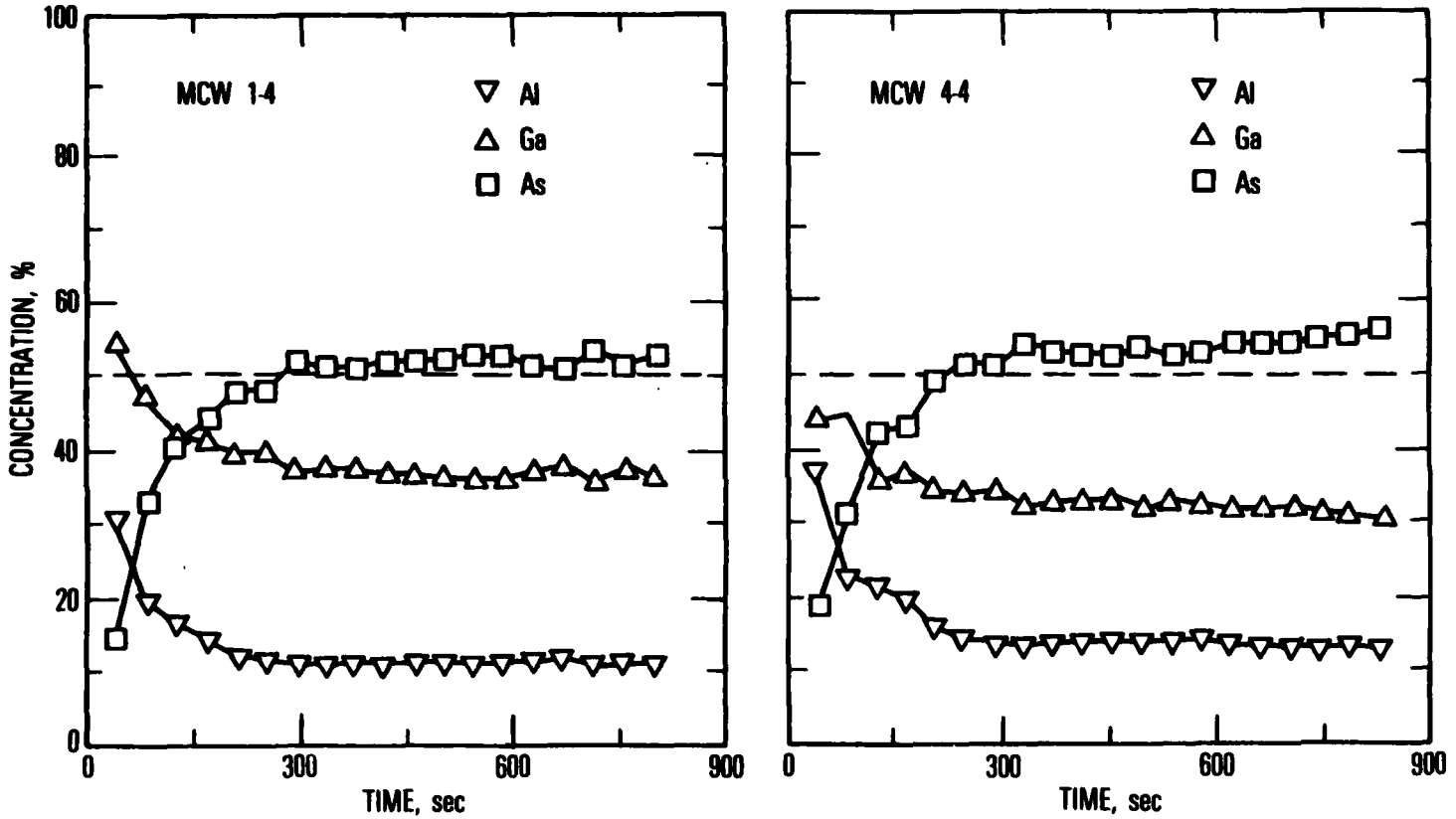

Figure 6. Determination by method II of percentage of Ga, Al, and As in samples MCW 1-4 and MCW 4-4 as a function of $^{18}O_2^+$ sputter etch time.

1. The $^{27}As^{+}$ ion current is very weak (on the order of 200 counts/sec). Although 5 sec is the total counting period, the low count rate leads to a rather large $^{27}As^{+}$ counting error of approximately $\mp 6\%$.

2. Competing reactions other than the formation of $^{27}As^{+}$ exist. These reactions include the formation of AsO^{+} with $^{18}O^{+}$, two $GaAs^{+}$ isomers with ^{69}Ga and ^{71}Ga, and negative As species. Because of the $^{27}As^{+}$ ion current of only a few hundred counts per second, even the smallest competing reaction changes the $^{27}As^{+}$ current by 5% to 10%.

3. For some samples the $^{27}As^{+}$ ion current never reaches a plateau with sputter etch time, whereas for every sample the $^{75}Al^{+}$ and $^{69}Ga^{+}$ ion currents reach plateaus. This phenomenon is an indication of As depletion near the surface and may have occurred because some of the layers remained in the hot hydrogen gas after growth.

V. PHOTOLUMINESCENCE

The optical excitation of carriers from the valence band to normally empty states in the conduction band results in sharp peaks in the photon emission that correspond to transitions from states near the bottom of the conduction band to states near the top of the valence band. This process is photoluminescence. Since the energy of the direct band gap in $Ga_{1-x}Al_xAs$ varies with the AlAs mole fraction X (Figure 7), the energy or wavelength of the photoluminescence peak measures the AlAs mole fraction in the crystal.

An experimental setup for room-temperature photoluminescence is shown in Figure 8. A Spectra Physics model 165 Ar laser is used to provide sample excitation with approximately 500 mW of power at 5145 Å. The peak wavelength of the luminescence is determined with a 0.25-m Jarrel-Ash monochromator to determine the peak wavelength. The laser light at 5145 Å is prevented from entering the monochromator by a filter.

The p- or n-dopant concentration varies the peak energy of the photoluminescence, and consequently the doping effect must be considered for a correct determination of the AlAs mole fraction X.

The carrier concentrations for p-type dopants with Ge in GaAs were determined by averaging several methods. The energy gap shrinkage ΔE_g is taken as the difference between 1.424 eV and the value of E_g measured by photoluminescence. The experimentally obtained expression[15]

$$p = \left(\Delta E_g / 1.6 \times 10^{-8} \right)^3 \qquad (12)$$

was used to calculate the concentration of p-type carriers. Additional calculations were based on the data of Kressel and Ettenberg,[16] which measured both the peak energy and the bandwidth at the half intensity of the photoluminescence of Ge-doped GaAs. Estimates from all of these references agreed to within a factor of two and agreed with the band-gap shift reported for Cd- and Zn-doped GaAs samples.[17]

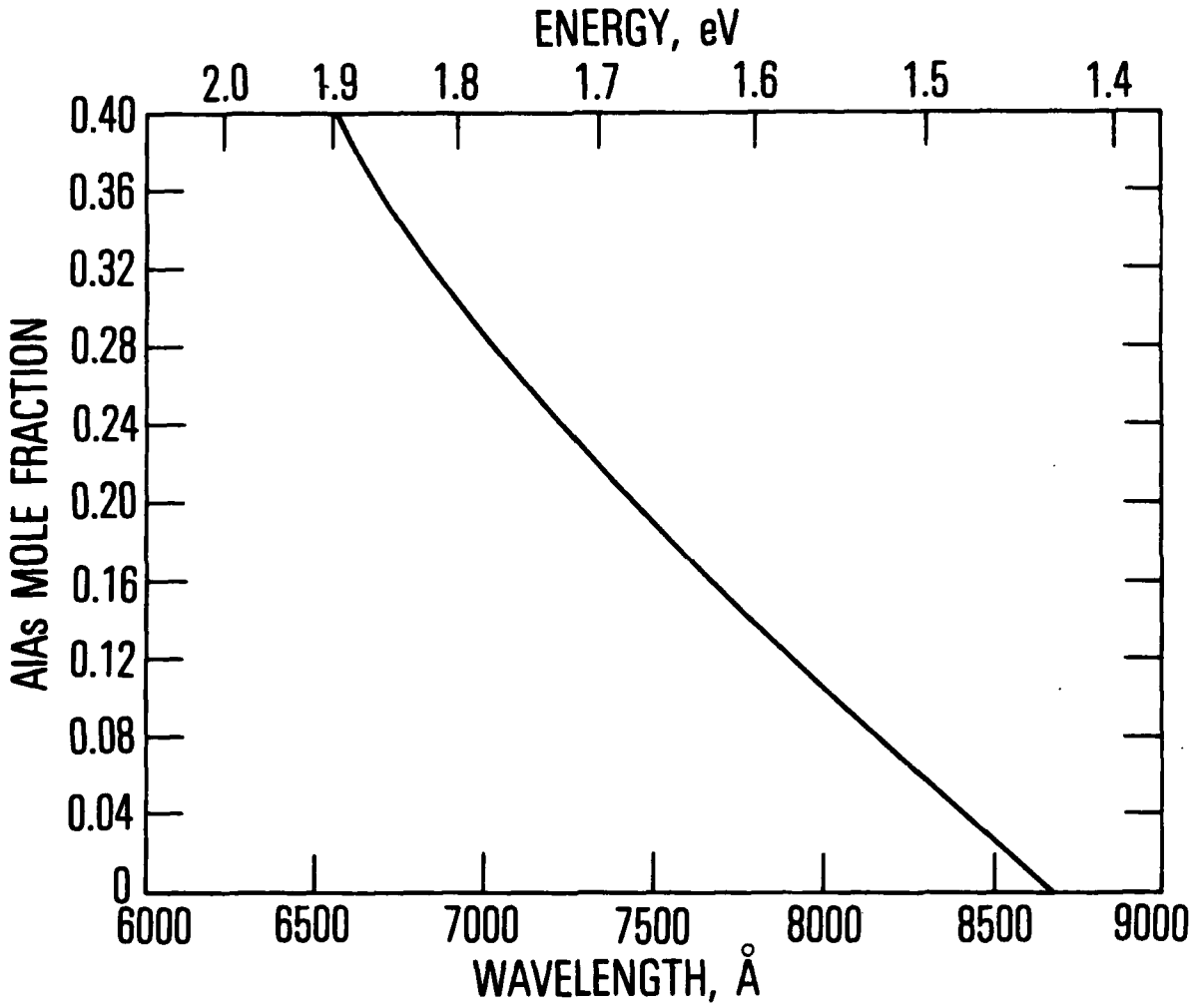

Figure 7. Dependence of photoluminescence peak energy on AlAs mole fraction for undoped $Ga_{1-x}Al_xAs$ layers.[19]

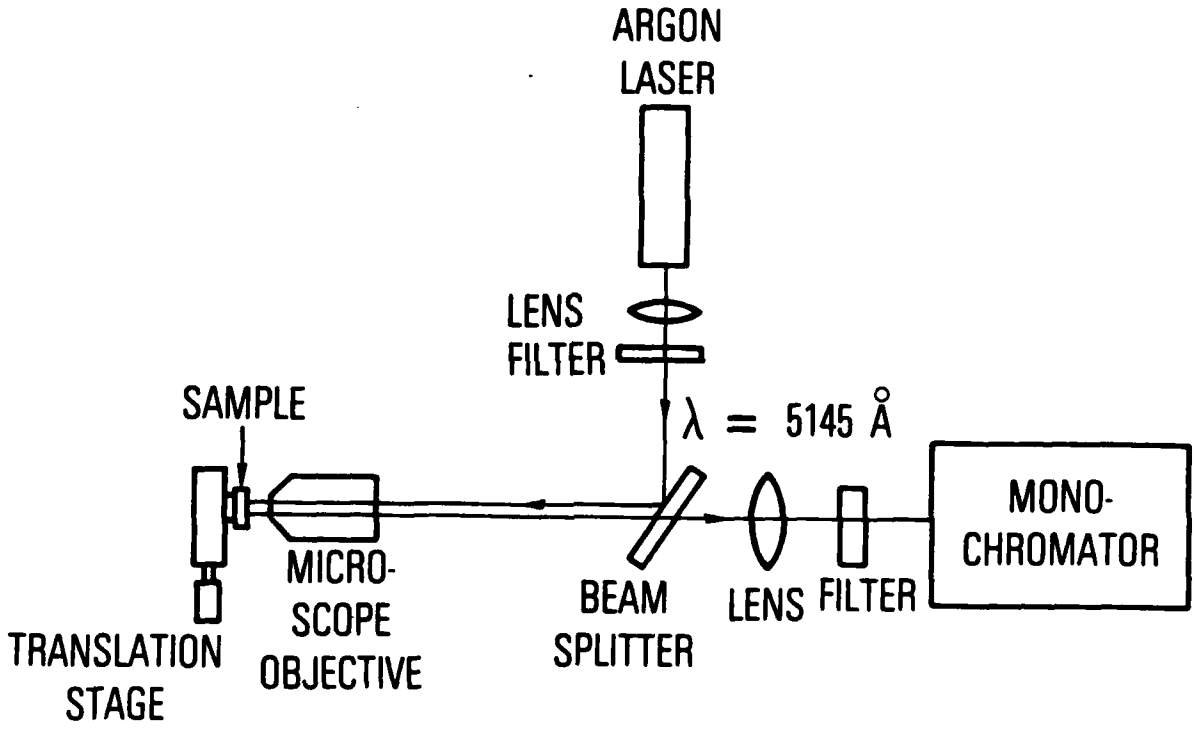

Figure 8. Photoluminescence setup used to determine AlAs mole fraction.

The carrier concentration for the n-type dopants with Te in GaAs was estimated from the energy gap shift reported for Se, Sn, and Te.[17]

Each of the five sets of doped samples was prepared with a fixed dopant mole percent in the melt solution. Therefore, within a sample set, the decrease in the LPE distribution coefficients[18,19] for the dopants with increasing AlAs mole fraction was accounted for in calculating the carrier concentrations of $Ga_{1-x}Al_xAs$ within the set. Once free carrier concentrations were determined, corrections for band-gap energy shifts were made, and the mole fraction X of AlAs for each sample was determined.

Photoluminescence data by Dingle et al.[19] gave the best agreement with Auger and IMMA and were used to determine the values of X reported in Table 1.

VI. DISCUSSION

Al concentrations as determined by the three characterization techniques and predicted by phase diagram data are tabulated in Table 1 for the six series of single-layer samples. The most likely explanation for why the phase diagram predictions are higher than the analytical results is that not all of the Al added to the melt may have been dissolved.

Auger analysis and ion microprobe mass analysis agree well for most of the samples. The agreement is good for both low and high Al concentrations and is independent of doping concentration and type.

The photoluminescence results agreed best with Auger analysis and IMMA results when the samples were not doped or when the AlAs composition was below 25% (IMMA). The worst agreement between photoluminescence and the other techniques occurred for the highly doped MCW 5 series. Photoluminescence is the least certain because it is dopant sensitive.

While Auger and IMMA are equally suited for Al analysis of single layers, Auger analysis would be the best technique for the Al analysis of $Ga_{1-x}Al_xAs$ multilayer structures. These structures are angle lapped at 2 deg to enlarge the exposed area of the layers by approximately 30 times. Thus, layers thicker than 1000 Å could be analyzed by Auger with a 3-μm electron beam diameter. Although the ion microprobe has a smaller beam diameter, the ion beam cannot remain stationary but must be rastered over a larger area to eliminate edge effects from the walls of the sputtered hole.

REFERENCES

1. M. B. Panish, S. Sumski, and I. Hayaski, "Preparation of Multilayer LPE Heterostructures with Crystalline Solid Solutions of $Al_xGa_{1-x}As$: Heterostructure Lasers," Metall. Trans. 2, 795 (1971).

2. J. M. Blum and K. K. Shih, "Growth of Smooth Uniform Epitaxial Layers by Liquid-Phase-Epitaxial Method," J. Appl. Phys. 43 (4), 1394 (1972).

3. L. R. Dawson, "Near-Equilibrium LPE Growth of GaAs-$Ga_{1-x}Al_xAs$ Double Heterostructures," J. Cryst. Growth 27, 86 (1974).

4. K. K. Shih, G. R. Woolhouse, A. E. Blakeslee, J. M. Blum, Inst. Phys. Conf. Ser. 24, 165 (1975).

5. M. B. Panish and M. Ilegems, Progress in Solid State Chemistry, Vol. 7, eds. H. Reiss and J. O. McCaldin, Pergamon, NY, 1969.

6. G. H. B. Thompson and P. A. Kirkby, "Liquid Phase Epitaxial Growth of Six-Layer GaAs/GaAl/As Structures for Injection Lasers with 0.04 μm Thick Centre Layer," J. Cryst. Growth 27, 70 (1970).

7. M. Ilegems and G. L. Pearson, "Derivation of the Ga-Al-As Ternary Phase Diagram with Applications to Liquid Phase Epitaxy," Proc. 2nd Int. Conf. on GaAs, Dallas, TX, p. 3 (1968).

8. M. B. Panish and S. Sumski, "Ga-Al-As: Phase, Thermodynamic and Optical Properties," J. Phys. Chem. Solids 30, 129 (1969).

9. H. C. Casey, Jr., and M. B. Panish, "Composition Dependence of the $Ga_{1-x}Al_xAs$ Direct and Indirect Energy Gaps," J. Appl. Phys. 40 (12), 4910 (1969).

10. J. R. Arthur and J. J. LePore. "Quantitative Analysis of $Al_xGa_{1-x}As$ by Auger Electron Spectroscopy," J. Vac. Sci. Technol. 14 (4), 979 (1977).

11. M. P. Seah and W. A. Dench, "Quantitative Electron Spectroscopy of Surfaces: A Standard Data Base for Electron Inelastic Mean Free Paths in Solids," Surface Interfac. Anal. 1 (1), 2 (1979).

12. E. B. Wilson, An Introduction to Scientific Research, McGraw-Hill, 1952.

13. R. Ludeke, L. Esaki, and L. L. Chang, "$Ga_{1-x}Al_xAs$ Superlattices Profiled by Auger Electron Spectroscopy," Appl. Phys. Lett. 24 (9), 417 (1974).

14. A. A. Van Oostrom, J. Vac. Sci. Technol. 13 (1), 224 (1976).

15. H. C. Casey, Jr., and F. Stern, "Concentration Dependent Absorption and Spontaneous Emission of Heavily Doped GaAs," J. Appl. Phys. 47 (2), 831 (1976).

16. H. Kressel and M. Ettenberg, "Electroluminescence and Photoluminescence of GaAs:Ge Prepared by Liquid Phase Epitaxy," Appl. Phys. Lett. 23 (9), 511 (1973).

17. P. D. Dapkus, N. Holonyak, Jr., J. A. Rossi, F. V. Williams, and D. A. High, "Laser Transition and Wavelength Limits of GaAs," J. Appl. Phys. 40 (8), 3300 (1969).

18. D. T. Cheung, Thesis, Stanford University, Stanford, California, Tech. Rept. 5124-1 (April 1975).

19. R. Dingle, R. A. Logan, and J. R. Arthur (unpublished).

LABORATORY OPERATIONS

The Laboratory Operations of The Aerospace Corporation is conducting experimental and theoretical investigations necessary for the evaluation and application of scientific advances to new military space systems. Versatility and flexibility have been developed to a high degree by the laboratory personnel in dealing with the many problems encountered in the nation's rapidly developing space systems. Expertise in the latest scientific developments is vital to the accomplishment of tasks related to these problems. The laboratories that contribute to this research are:

Aerophysics Laboratory: Launch vehicle and reentry aerodynamics and heat transfer, propulsion chemistry and fluid mechanics, structural mechanics, flight dynamics; high-temperature thermomechanics, gas kinetics and radiation; research in environmental chemistry and contamination; cw and pulsed chemical laser development including chemical kinetics, spectroscopy, optical resonators and beam pointing, atmospheric propagation, laser effects and countermeasures.

Chemistry and Physics Laboratory: Atmospheric chemical reactions, atmospheric optics, light scattering, state-specific chemical reactions and radiation transport in rocket plumes, applied laser spectroscopy, laser chemistry, battery electrochemistry, space vacuum and radiation effects on materials, lubrication and surface phenomena, thermionic emission, photosensitive materials and detectors, atomic frequency standards, and bioenvironmental research and monitoring.

Electronics Research Laboratory: Microelectronics, GaAs low-noise and power devices, semiconductor lasers, electromagnetic and optical propagation phenomena, quantum electronics, laser communications, lidar, and electro-optics; communication sciences, applied electronics, semiconductor crystal and device physics, radiometric imaging; millimeter-wave and microwave technology.

Information Sciences Research Office: Program verification, program translation, performance-sensitive system design, distributed architectures for spaceborne computers, fault-tolerant computer systems, artificial intelligence, and microelectronics applications.

Materials Sciences Laboratory: Development of new materials: metal matrix composites, polymers, and new forms of carbon; component failure analysis and reliability; fracture mechanics and stress corrosion; evaluation of materials in space environment; materials performance in space transportation systems; analysis of systems vulnerability and survivability in enemy-induced environments.

Space Sciences Laboratory: Atmospheric and ionospheric physics, radiation from the atmosphere, density and composition of the upper atmosphere, aurorae and airglow; magnetospheric physics, cosmic rays, generation and propagation of plasma waves in the magnetosphere; solar physics, infrared astronomy; the effects of nuclear explosions, magnetic storms, and solar activity on the earth's atmosphere, ionosphere, and magnetosphere; the effects of optical, electromagnetic, and particulate radiations in space on space systems.